Plasma Sources Sci. Technol. **17** (2008) 025001 (10pp) doi:10.1088/0963-0252/17/2/025001

Influence of magnetic field and discharge voltage on the acceleration layer features in a Hall effect thruster

D Gawron[1], **S Mazouffre**[1], **N Sadeghi**[2] **and A Héron**[3]

[1] ICARE, CNRS, 1C Avenue de la Recherche Scientifique, 45071 Orléans, France
[2] LSP, Université Joseph Fourier - CNRS, 38402 Saint Martin d'Hères, France
[3] CPHT, École Polytechnique, F91128 Palaiseau, France

E-mail: stephane.mazouffre@cnrs-orleans.fr

Received 6 July 2007, in final form 4 December 2007
Published 10 March 2008
Online at stacks.iop.org/PSST/17/025001

Abstract
The axial velocity of singly charged xenon ion is determined by means of laser induced fluorescence spectroscopy at the exhaust of a PPS100-LM Hall effect thruster by analyzing the Doppler shifted spectral profile of the 834.72 nm Xe^+ ion line. Measurements are carried out both inside and outside the thruster channel. Ion velocity distribution functions (VDF) are used to compute the ion accelerating potential. It is shown that such a potential can in fact be defined in several ways due to the overlap between the ionization and acceleration layers, which translates into broad VDF. The PPS100-LM thruster is operated under an applied voltage ranging from 100 to 300 V and a magnetic field produced by coils whose current is varied from 2.5 to 5.5 A. The broad range of working conditions allows one to determine the influence of these two parameters on the ion dynamics. Finally, the experimental results are used to confirm the outcomes of a 2D kinetic model.

(Some figures in this article are in colour only in the electronic version)

1. Introduction

In the field of space propulsion, electric propulsion is the most efficient way to reduce the amount of propellant necessary to achieve a given velocity increment as the electrostatic acceleration of an ionized propellant allows a high exhaust velocity to be reached [1]. Nowadays, the two most mature technologies are the gridded ion engine and the Hall effect thruster (HET). The latter inherits a long successful flight history from the Soviet/Russian space program, which has flown the stationary plasma thruster (SPT) variant since 1972 [2]. The implementation of Hall thrusters on Western satellites is now underway [3–5]. Moreover, the recent success of the SMART-1 mission to the Moon, from the European Space Agency, demonstrates that HETs are good candidates for long duration missions [3,8]. The interest in HET is related to several features of this specific thruster design [6,7]:

– a much higher specific impulse (>1500 s) in comparison with chemical thrusters (<500 s) with a thrust efficiency in excess of 50%, a thrust level ∼100 mN and a lifetime >5000 h at 1.5 kW electric power,
– a relatively simple and robust design that provides gridless acceleration of the ion flow and
– a dual-mode operation capability, i.e. either a large thrust or a high specific impulse regime.

The goal of this work is the characterization of the ion transport properties in a laboratory model of a PPS100 HET by means of laser induced fluorescence (LIF) spectroscopy. The PPS100-LM behavior is studied for discharge voltages ranging from 100 to 300 V with 100 V increment and for coil currents varying between 2.5 and 5.5 A with 1.0 A increment. Experimental Xe^+ ion velocity distribution functions (VDF) are compared with the outcomes of hybrid and kinetic simulations.

LIF spectroscopy has already been extensively used in the past few years [9, 10], but even though this diagnostic tool allows the measurements of the ion VDF, more often than not, only the most probable velocity and the mean velocity are mentioned in papers. This study focuses on the shape and

 © 2008 IOP Publishing Ltd Printed in the UK

properties of the measured VDF, without using a deconvolution method [11], in order to bring to light the relationship between the ionization and acceleration layers and subsequent impact on ion transport phenomena. Moreover, to the best of our knowledge, this is the first time that the way to derive the accelerating potential and the electric field distributions from measured ion VDFs is questioned.

2. Laser induced fluorescence

LIF is a non-intrusive diagnostic tool that enables one to determine the velocity of probed particles along the laser beam direction by measuring the Doppler shift of absorbed photons. The transition used in the measurements presented in this paper is the $5d\ ^2F_{7/2} \longrightarrow 6p\ ^2D^o_{5/2}$ at $\lambda_{air} = 834.723$ nm, which has been chosen due to a large population in the $5d\ ^2F_{7/2}$ metastable state of Xe^+ and due to the favorable branching ratio of the $\lambda_{air} = 541.915$ nm line originating from its upper state that allows non-resonant LIF. Measuring the frequency at which the laser beam energy is absorbed allows one to determine the ion Doppler shift. Therefore, it is possible to calculate the ion velocity component corresponding to the laser beam direction by using the following equations:

$$\Delta\nu = \nu - \nu_0 = \frac{1}{2\pi}\boldsymbol{k}\cdot\boldsymbol{v} \quad \text{and} \quad v_k = c\frac{(\nu - \nu_0)}{\nu}, \qquad (1)$$

where $\Delta\nu$ is the Doppler shift, $\boldsymbol{k}$ is the laser beam wave vector, $\boldsymbol{v}$ is the ion velocity vector, c is the speed of light, v_k is the ion velocity parallel to $\boldsymbol{k}$, ν_0 is the studied transition unshifted frequency and ν is the recorded frequency. We have made our own precise measurement of the absolute value of λ_0 in a low-pressure stationary xenon plasma: $\lambda_0 = (834.7233 \pm 0.0001)$ nm [12].

Even though a LIF signal is a convolution of the VDF with the absorption line shape and the laser frequency profile [11], VDFs presented in this paper correspond to raw profiles. The relative frequency shift of the 19 isotopic and hyperfine components of the transition is still mostly unknown [13]. The Zeeman splitting cannot be accounted for in the region of strong magnetic field. As a consequence, the uncertainty of the deconvolution procedure outcome is too large to bring any benefit in terms of information about the exact VDF shape and width. As measured in a low-pressure RF discharge the width of the Xe^+ ion VDF is around 600 MHz at 300 K whereas it is typically above 2 GHz in the plasma of the PPS100-LM thruster [12]. The effect of broadening mechanisms is in fact so important, as we will see in section 4, that no deconvolution is necessary. LIF provides the complex profile resulting from the convolution of VDF and absorption lineshape as long as none of the isotopic and hyperfine components of the transition is saturated. With a chosen power density below 1 mW mm^{-2}, we are confident that our measurements are not spoiled by saturation effects, all the more because the interaction time between the laser beam and ions is reduced inside and outside a HET [14].

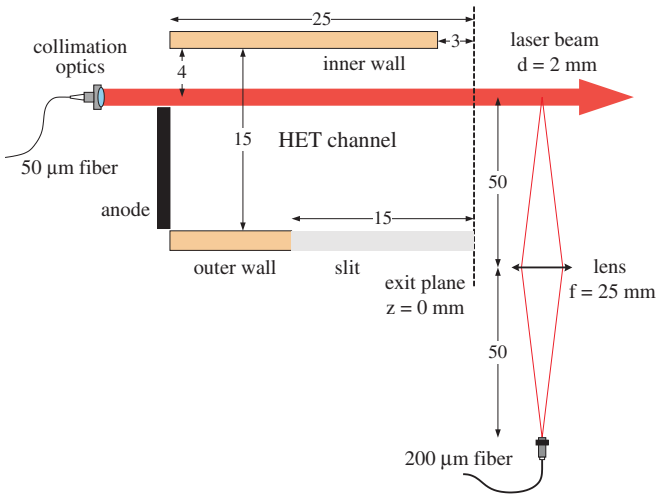

Figure 1. Schematic drawing of the laser injection into the PPS100 channel and of the detection branch. The unit of dimensions is mm.

3. Experimental setup

The studied thruster is a laboratory model of a 1.5 kW-class Snecma-built thruster, the so-called PPS100-LM, whose design and dimensions are close to those of the SPT100 thruster developed by Fakel. The channel is 25 mm in length; the inner and outer dielectric walls are 70 mm and 100 mm in diameter, respectively. A hole 2 mm in diameter is bored through the thruster rear elements so that a laser beam can be shot into the discharge chamber parallel to the channel axis, as shown in figure 1. The laser beam axis is 4 mm from the internal wall. The external wall has a slit parallel to the thruster axis from the exit plane to 15 mm inside the channel in order to be able to collect the Xe^+ ion fluorescence signal inside the channel (see figure 1). In the remainder of this contribution, the exit plan is used as a reference; therefore it corresponds to $z = 0$ mm.

The optical bench was extensively described elsewhere [12]. In summary, the laser beam used to excite Xe^+ metastable ions, thus providing the fluorescence radiation at 541.9 nm, is produced by a single-mode external cavity laser diode (Sacher TEC 500) scanned over the 834.7 nm Xe^+ line. The laser remains mode-hop free over a frequency tuning range of more than 10 GHz without current–voltage coupling. The laser beam passes through a Faraday isolator to prevent optical feedback into the laser cavity, and through a series of beam splitters to generate secondary beams used to monitor the laser power and wavelength. The wavelength is accurately measured by means of a calibrated WS/8UV wavemeter from HighFinesse whose absolute accuracy is better than 100 MHz, which corresponds to $\sim$90 m s^{-1}. The measurement is backed up by a NO_2 gas cell and a Fabry–Pérot interferometer, which act as failsafe devices. The primary laser beam is modulated by a mechanical chopper before being coupled into a 60 m long multi-mode optical fiber of 50 μm core diameter. The fiber allows the passage of the laser beam into the vacuum chamber of the ground-test facility. The fiber output is located behind the thruster. Collimation optics are used to form a $\sim$2 mm in diameter beam that passes through the hole at the back of the thruster. The laser beam propagates

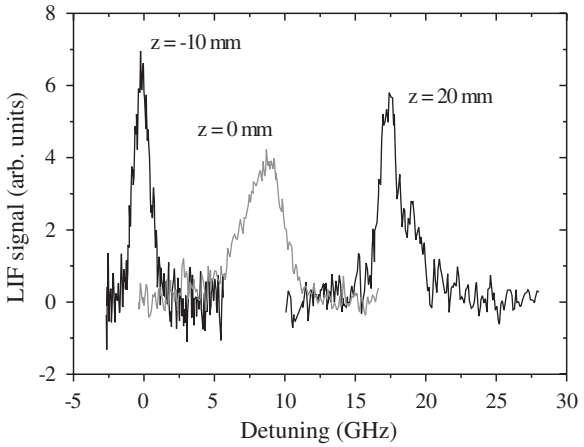

Figure 2. Ion axial VDF at various positions along the channel axis for $U_d = 200$ V, $I_c = 4.5$ A and $\phi_a = 5$ mg s^{-1}.

parallel to the channel axis in the direction of the ion flow (see figure 1). A detection branch made of a 25.4 mm focal length, which focuses the fluorescence light onto a 200 μm core diameter optical fiber, is mounted onto a translation stage perpendicular to the channel axis, as shown in figure 1. The magnification ratio is unity meaning that the spatial resolution is 200 μm in the axial direction. The collection system allows probing an area stretching from 15 mm into the channel up to 30 mm downstream of the channel exit plane. The light is transported by way of the 200 μm fiber to a 20 cm focal length monochromator that isolates the 541.9 nm line from the rest of the spectrum. A Hamamatsu R928 photomultiplier tube serves as a light detector. A lock-in amplifier operating at the chopper frequency is used to discriminate the fluorescence light from the intrinsic plasma emission.

The PPS100-LM thruster is operated at several operating conditions. The applied voltage U_d is varied from 100 to 300 V in 100 V steps. The magnetic field is varied by changing the current I_c flowing in the coils from 2.5 to 5.5 A in 1 A increments. I_c is kept fixed at 4.5 A when changing U_d. In a like manner, U_d is kept constant at 200 V when changing I_c. For all these operating conditions the anode xenon mass flow rate stays unchanged at 5 mg s^{-1}. The cathode gas flow rate is 0.4 mg s^{-1} for all series. Results are also reported in [12] about another operating condition that exhibits a low level of discharge current oscillations: $U_d = 275$ V, $I_c = 3.8$ A and $\Phi_a = 3$ mg s^{-1}.

4. Analysis of the Xe$^+$ ion VDF

LIF measurements allow one to monitor the component of the Xe$^+$ ion VDF along the laser beam propagation axis, i.e. in the axial direction. Before trying to derive from the measurements a quantity that characterizes the ion velocity both inside and outside the channel, one must analyze the shape of the measured Xe$^+$ VDFs. A few examples of ion VDF recorded at a 200 V applied voltage are given in figure 2. In this figure it is clearly visible that the width of the VDF varies along the channel axis. In other words, the dispersion in the Xe$^+$ ion axial velocity changes when moving downstream. In order to characterize this phenomenon, let us define a p parameter calculated from the second order moment of the distribution function so that p is equal to the FWHM in the case of a Gaussian distribution [12]. The p quantity reads

$$p = 2\sqrt{2\ln(2)}\sigma = 2\sqrt{2\ln(2)}\sqrt{\frac{\int (v-\bar{v})^2 \mathrm{VDF}(v)\,\mathrm{d}v}{\int \mathrm{VDF}(v)\,\mathrm{d}v}}, \quad (2)$$

where σ is the dispersion and $\bar{v}$ is the mean velocity inferred from the first order moment of the VDF. The quantity p characterizes the spread in ion velocity; it is expressed in m s^{-1}. The ion energy dispersion in eV is related to p by

$$\Delta E = m_{\mathrm{Xe}^+} \times \bar{v} \times p, \quad (3)$$

where m_{Xe^+} is the ion mass. The ion velocity dispersion increases from the back of the channel up to an area located ahead of the channel exit plane before it decreases toward a non-zero value in the far field, as can be seen in figures 3 and 4. The amplitude of the dispersion depends on the thruster working conditions; however, the order of magnitude is of a few thousand m s^{-1}, i.e. several tens of eV. Moreover, as can be seen in figure 2, a low velocity wing appears on the VDFs inside the channel close to the outlet ($z \approx 0$ mm). Far from the exit plane ($z > 20$ mm), the low velocity wing almost vanishes whereas a high velocity wing shows up. The most plausible explanation for the formation of a 'slow wing' on the Xe$^+$ ion VDF in the vicinity of the channel exhaust is the creation of low velocity ions within the acceleration layer. The latter is defined as the zone through which the potential drops, i.e. the zone through which ions experience acceleration. In a HET, an overlap exists between the ionization and the acceleration layers [16, 15]. The energy gain within this last layer differs for ions created at different locations. Inside the channel and in the plume near field ($z \leqslant$ 10–15 mm), the addition of slow ions formed ahead of the observation point broadens the VDF. In the far field ($z \geqslant$ 10–15 mm), Xe$^+$ ions created within the acceleration zone exhibit a low axial velocity as they did not experience the complete potential drop. The p parameter then reaches the highest value where the ionization layer ends. Beyond this point, the ion energy dispersion corresponds to the mean energy difference between partly and fully accelerated ions [12]. As a consequence, p decreases as Δv scales like $\Delta E/\bar{v}$, see equation (3).

Such an evolution of the VDF with z has also been observed by Hargus, who considers the charge exchange reaction between Xe atoms and Xe$^+$ ions as an explanation for the broadening of the ion VDF. However, with a charge exchange cross section of 6×10^{-19} m^2 [17] and a Xe atom density of 5×10^{18} m^{-3} inside the channel of a PPS100 operating at normal conditions (see e.g. [16]), the calculated mean free path of Xe$^+$ ions is 0.33 m. This makes negligible the charge exchange probability within the last 5 mm in the channel, where an important fraction of the potential drop occurs. Outside the channel, where Xe$^+$ ions gain the major part of their final kinetic energy, the neutral density is around 10^{17} m^{-3}, which leads to a mean free path of several meters. All these together make negligible the contribution of the charge exchange process to the observed broadening of the

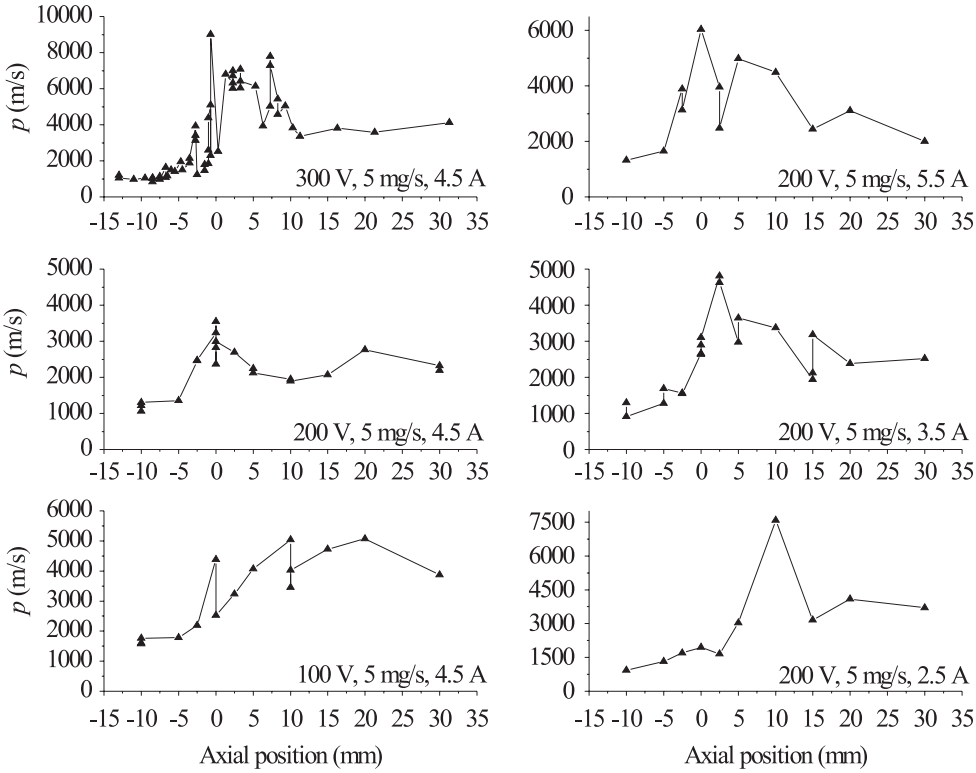

Figure 3. Development along the axis of the velocity dispersion (p parameter) when changing the applied voltage and the magnetic field.

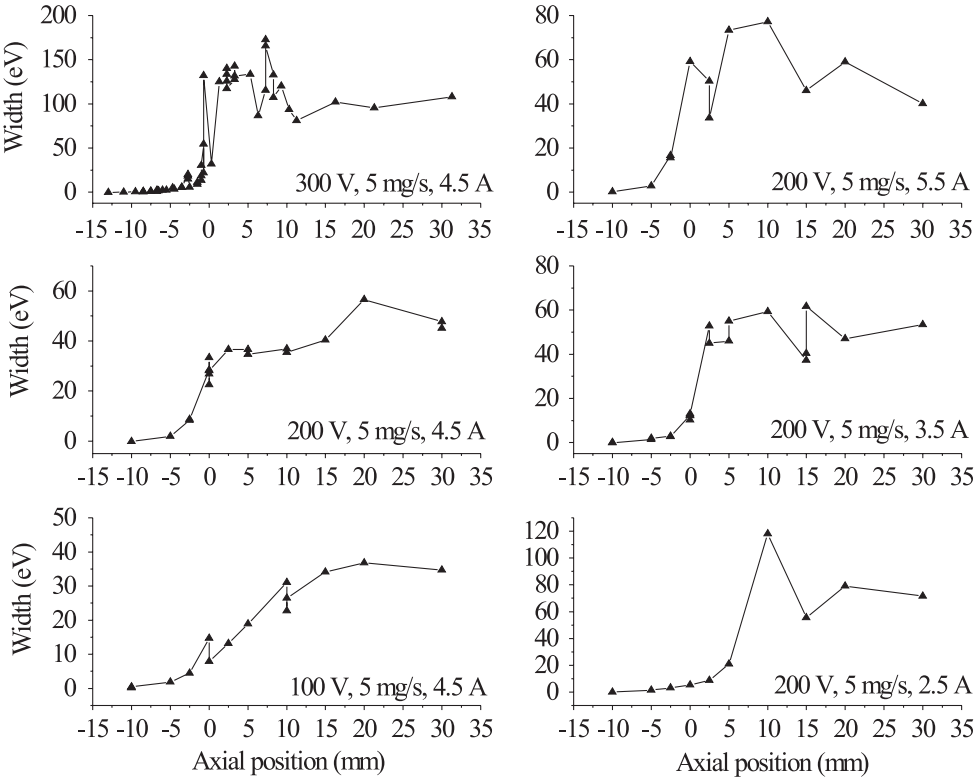

Figure 4. Development along the axis of the dispersion in kinetic energy when changing the applied voltage and the magnetic field.

VDFs. Another point is in favor of our explanation. The metastable Xe atom behavior has been monitored under the same experimental conditions by means of laser spectroscopy. The $6s'\ [1/2]^0_1 \longrightarrow 6p'\ [3/2]_2$ transition was pumped at $\lambda_{air} = 834.6823$ nm and the fluorescence yield was recorded at $\lambda_{air} = 473.415$ nm [12]. Even though atom velocity dispersion increases slightly along the channel axis, it always remains close to the thermal speed. Besides, the atom VFD does not

display a high velocity wing that would be caused by charge exchange with accelerated ions. In like manner, no fast atoms were detected. However, it is worth noting that the properties of metastable and ground-state Xe atoms could be different.

Low-frequency plasma oscillations, so-called 'breathing mode' oscillations at ∼15–20 kHz [16, 18], can also have an impact upon the VDF shape. Breathing mode oscillations correspond to a prey–predator-type process, and therefore they lead to a displacement of the ionization front inside the channel [19, 20]. Ions created within the acceleration layer at various instants experience a different potential drop as the ionization layer moves back and forth. First, the velocity dispersion of a time-averaged Xe^+ ion VDF should be larger than the one of an instantaneous VDF [20]. Moreover, as revealed by computer simulations in which the acceleration layer properties can be changed, the time-averaged ion VDF is broader when low-frequency plasma oscillations are considered as they dictate the length over which the ionization and acceleration layers overlap [12]. However, plasma oscillations alone cannot induce any velocity dispersion if the two zones never overlap [12].

5. Minimum and maximum ion velocity

Classically, either the most probable velocity or the mean velocity are used to characterize the ion velocity in a HET [11]. Nevertheless, these two quantities do not give information about the VDF shape. Besides, neither experimentally measured mean velocity nor most probable velocity provide enough information so that comparisons with numerical simulations of ion transport phenomena are relevant. In this work we propose to consider the slowest and the most rapid ions as well. Indeed, the former experience the tiniest fraction of the potential drop whereas the latter experience the full potential drop. Thus, in addition to the ion mean velocity, which in our measurements always matches the most probable velocity, let us define the so called minimum and maximum velocities $v_{\min}$ and $v_{\max}$. The $v_{\min}$, respectively, $v_{\max}$, quantity corresponds to the velocity for which the amplitude of the distribution drops to 10% of its maximum value on the low, respectively high, velocity side, as shown in figure 5. The arbitrary 10% factor is chosen to warrant an unambiguous definition of both $v_{\min}$ and $v_{\max}$ as the poor S/N ratio enables one to accurately determine the true minimum and maximum velocity from the measured VDFs.

The quantities $v_{\min}$ and $v_{\max}$ are complementary to the p parameter and give extra information about the ion flow properties. As can be seen in figure 6, $v_{\max}$ is of particular interest. For almost all studied experimental conditions, $v_{\max}$ reaches, in the plume far field, the theoretical maximum velocity $v_{\mathrm{th,max}}$ defined as

$$v_{\mathrm{th,max}} = \sqrt{\frac{2eU_{\mathrm{d}}}{m_{\mathrm{Xe^+}}}}. \tag{4}$$

Under normal operating conditions of the PPS100 thruster, i.e. 300 V applied voltage and 4.5 A current flowing through

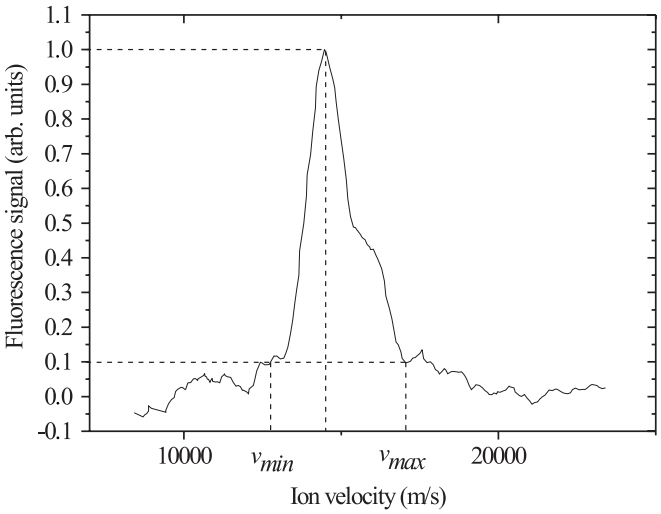

Figure 5. Definition of $v_{\min}$ and $v_{\max}$.

the coils, $v_{\max}$ is even higher than $v_{\mathrm{th,max}}$. The existence of Xe^+ ions with a kinetic energy higher, or even much higher, than the applied potential energy has also been observed by retarding potential analyzer measurements [12,21]. Moreover, experimental data are in qualitative agreement with numerical outcomes of hybrid and PIC models [19, 20, 15]. This peculiar phenomenon can be explained by the effect of so-called ion transit-time oscillations of which the frequency range ∼100–500 kHz corresponds to the reciprocal of the time necessary for ions to cross the acceleration zone. The origin of ion transit-time oscillations is still ill-understood; however, computer simulations predict their presence [15, 19], and hints of their existence have been experimentally observed [22,23]. Transit-time oscillations can be seen as the oscillation in space and in time of the electric field. For the sake of clarity, let us simply consider the case in which the electric field solely moves back and forth at high frequency. When the potential profile moves upstream, ions created close to the channel exit have less and less potential energy that can be converted into kinetic energy, hence the appearance of very slow ions. On the contrary, when the potential moves downstream, ions that were already inside the acceleration layer have the possibility to gain an extra amount of energy. Thus, the kinetic energy of a fraction of Xe^+ ions can be higher than the applied potential energy, as can be seen in figure 6. Identical conclusions can be drawn from oscillations in time of the electric field.

As shown in figure 7, the ion VDFs measured in the plume far field by means of RPA with a grounded entrance grid reveal as well the existence of very slow and very fast ions. For instance, some Xe^+ ions possess a kinetic energy of 450 eV and others have an energy below 200 eV whereas the applied voltage is 300 V.

6. Local potential extraction

As a significant fraction of ions are created within the acceleration layer, extracting the energy deposited into the propellant from v_{mean} would furnish an underestimated value since v_{mean} accounts for fully and partly accelerated ions.

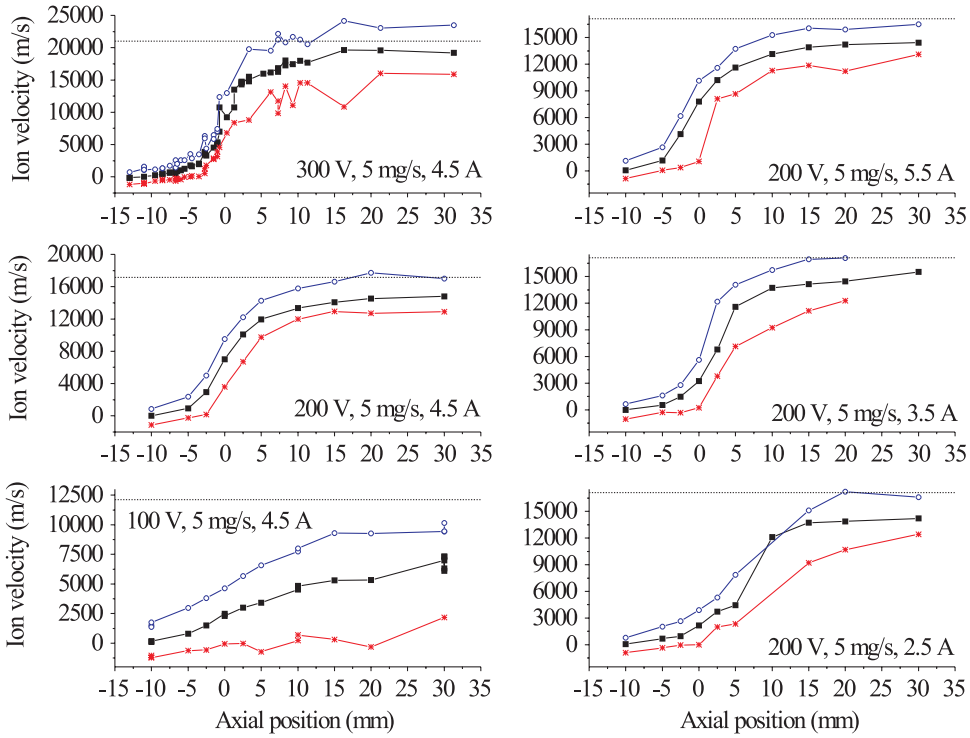

Figure 6. Distribution of the ion axial velocity along the channel axis for several thruster working conditions: mean velocity (■), maximum velocity (●) and minimum velocity (∗).

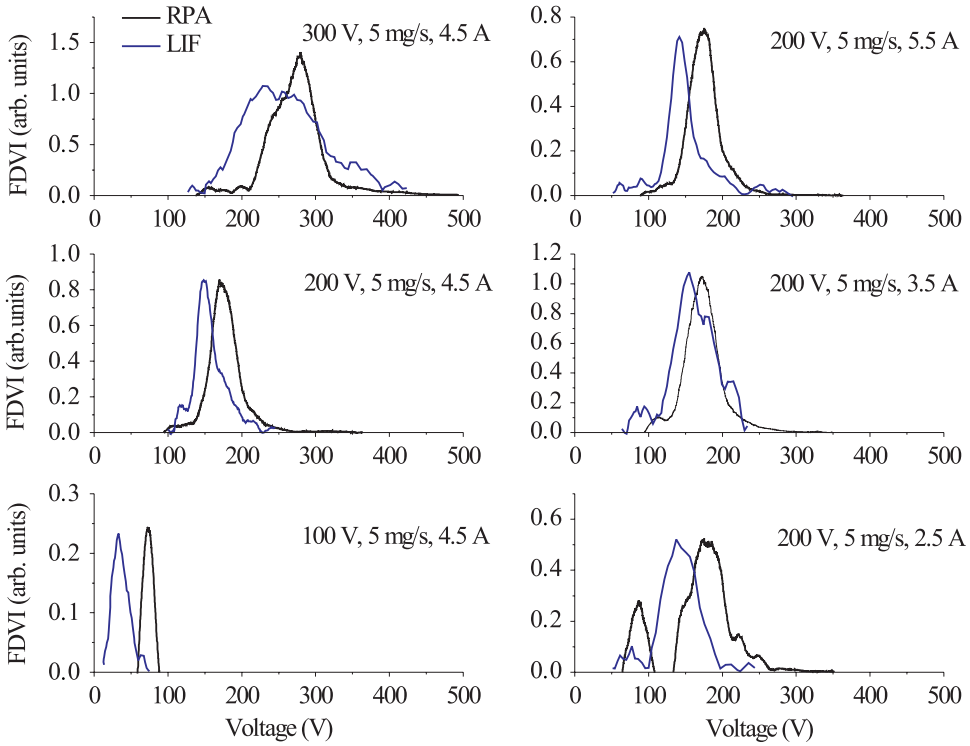

Figure 7. Xe^+ ion VDF measured at $z = 30$ mm by means of LIF (grey line) and at $z = 700$ mm by means of RPA (black line). The HET operating conditions are changed. The observed shift in potential is due to the fact that the RPA is grounded [12].

Therefore, the use of v_{max} instead of v_{mean} would provide a more realistic value of the acceleration potential as the fastest ions have necessarily undergone the full potential drop. However, when the effect of electric field oscillations is not negligible, the fastest ions gain more than the applied potential, as previously shown. Thus another reason to discard 10% of the most rapid ions is to attenuate the effect of transit-time oscillations on our estimation of the acceleration potential.

Figure 8 displays the local potentials extracted from v_{mean} and v_{max} for six different working conditions. The plot

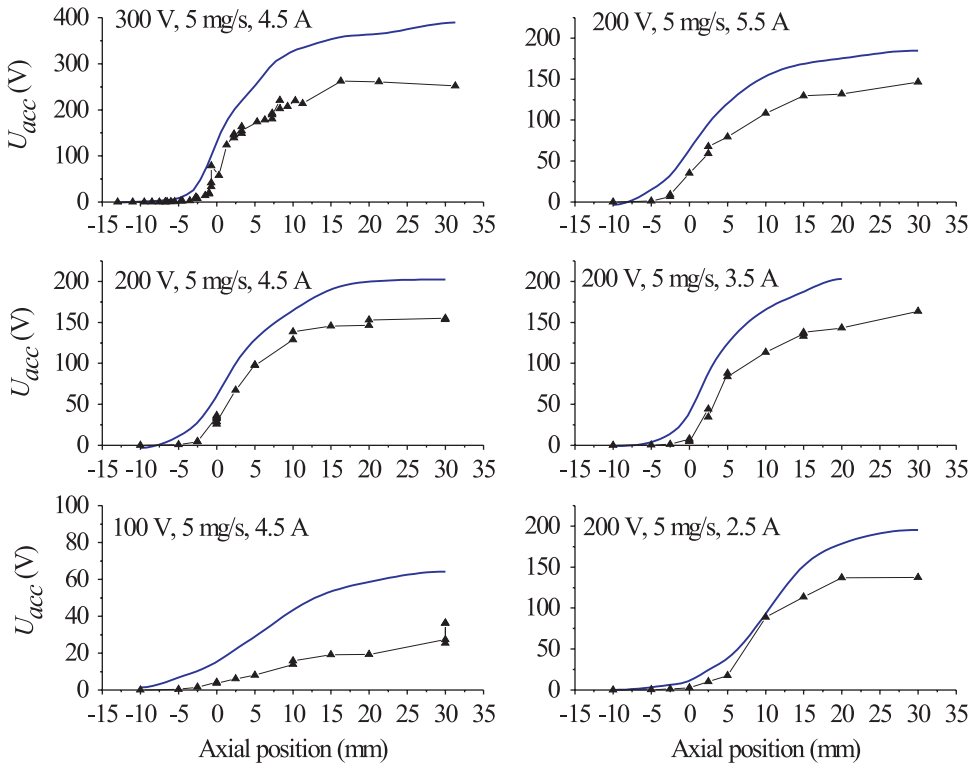

Figure 8. On-axis development of the ion accelerating potential. Potential profile obtained from v_{mean} (▲). Potential profile obtained from v_{max} (——).

Table 1. Evolution of the fraction of the accelerating potential inside the thruster channel for various PPS100 thruster operating parameters. The quantity ΔU is obtained from equation (5). The subscripts mean and max refer to the mean ion velocity and the maximum ion velocity, respectively.

Change of U_d ($\phi_a = 5\,mg\,s^{-1}$, $I_c = 4.5\,A$)			Change of B ($\phi_a = 5\,mg\,s^{-1}$, $U_d = 200\,V$)		
U_d (V)	ΔU_{max}	ΔU_{mean}	I_c (A)	ΔU_{max}	ΔU_{mean}
100	0.23	0.14	2.5	0.05	0.02
200	0.28	0.17	3.5	0.20	0.03
300	0.30	0.23	4.5	0.28	0.17
			5.5	0.33	0.24

that corresponds to normal working condition ($U_d = 300\,V$, $I_c = 4.5\,A$, $\Phi_a = 5\,mg\,s^{-1}$) displays a potential which is about 100 eV higher than U_d in the far field when v_{max} is used. This suggests that transit-time oscillations are quite active at the optimal regime of a HET [18]. In such a case, the true local potential would lie somewhere between the potential calculated from v_{mean} and the one obtained from v_{max}. Table 1 shows the fraction of accelerating potential ΔU inside the thruster channel calculated from either v_{mean} or v_{max}. The quantity ΔU is calculated as follows:

$$\Delta U = \frac{U_{z=0\,mm}}{U_{z=30\,mm}}, \tag{5}$$

from data displayed in figure 8. As can be seen in figure 8 and in table 1, the potential calculation method impacts greatly onto the percentage of energy deposited into the propellant. The definition of a correct potential profile is not obvious, as it strongly depends upon processes accounted for. However, we believe that the potential assessed from v_{max} is the most appropriate since the overlap between the acceleration and the ionization layers does not have a significant influence on v_{max}. As shown in table 1, the percentage of energy deposited into the propellant inside the channel increases with U_d and I_c. The percentage of potential inside the channel increases from 5% to 33% when I_c varies from 2.5 to 5.5 A, that means when the magnetic field strength rises. Likewise, it increases from 23% to 30% when U_d is varied from 100 to 300 V.

Let us first discuss the trend when U_d is fixed and B increases. The anomalous electron mobility μ_e is proportional to $1/B$, hence the efficient electron trapping within the magnetic barrier of a HET. As μ_e decreases when B increases, the axial electric field E_z is mainly located in the vicinity of the channel exit, i.e. in the area where B is maximum, as can be seen in figure 9. The electric field curve is directly obtained from calculation of the derivative of the potential profile, the latter being inferred from the velocity distribution along the channel axis. Under normal condition, E_z reaches up to $400\,V\,cm^{-1}$ at the channel exit. When changing the current flowing into the coils, both the magnetic field magnitude and gradients vary. The two quantities increase with I_c. The region through which B is strong enough to trap electrons then expands with I_c. Therefore, the zone over which the electric field E_z does exist also expands and the mean value of E_z decreases (when U_d is kept constant), in compliance with experimental data shown in table 2. The averaged value of the electric field as well as its spatial extent are presented in table 2. The spatial extent of E_z corresponds to the ratio of U_{max} to $\bar{E}_z$ where U_{max} is the maximum value of

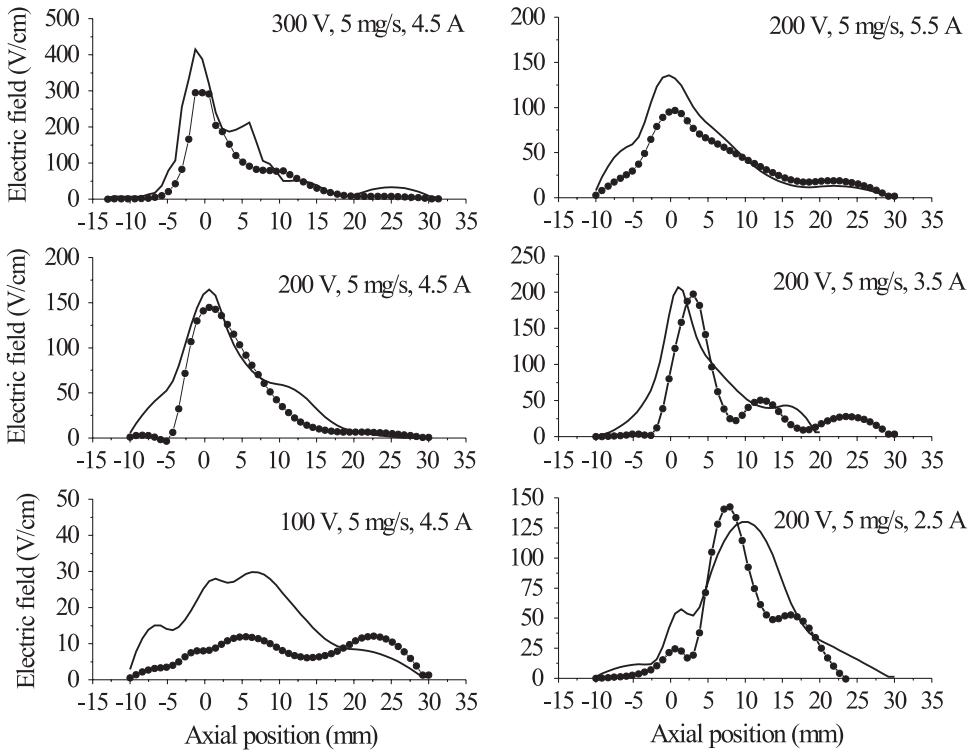

Figure 9. Electric field along the channel axis for various conditions. Calculation based on v_{mean} (●). Calculation based on v_{max} (——).

the measured accelerating potential, see figure 8. Note that the uncertainty is large for $I_c = 2.5$ A as the spatial resolution of the corresponding velocity profile is poor in the steep gradient region, see figure 6. A direct consequence of the expansion of the electric field with I_c is the increase in the length of the acceleration layer inside the channel. Hence, the percentage of energy deposited into the propellant inside the thruster rises with B. This assertion correlates with the rise of the dispersion of the Xe^+ ion VDF at the channel exit when I_c increases and U_d is fixed, see figures 3 and 4.

Analyzing the case with fixed B and changing U_d is also instructive. A first impact is the increase of the dispersion in velocity of the Xe^+ ions with U_d, as can be seen in figures 3 and 4. Another effect is the upstream shift of the potential profile when the applied voltage is increased. One way to explain this fact is to consider the evolution of the electron energy. When the potential is ramped up, the electron temperature increases [24]. As a consequence, the electron confinement within the magnetic field becomes less efficient. Electrons penetrate deeper into the channel, hence an upstream motion of the potential drop. Moreover, the zone over which electrons are trapped narrows down as confirmed by data shown in table 2. The spatial extent of the electric field decreases when U_d is ramped up.

Table 2. Averaged electric field $\bar{E}_z$ and spatial extent of the electric field δE_z for various operating conditions when E_z is obtained from the v_{max} data set. The quantity δE_z is the ratio of U_{max} to $\bar{E}_z$ where U_{max} is the maximum value of the measured accelerating potential.

Change of U_d			Change of B		
U_d (V)	$\bar{E}$ (V cm^{-1})	δE (cm)	I_c (A)	$\bar{E}$ (V cm^{-1})	δE (cm)
100	15	4.3	2.5	48	4.1
200	57	3.5	3.5	67	3.0
300	133	2.9	4.5	57	2.5
			5.5	46	4.0

7. Comparison with implicit model outcomes

In the past few years, several models simulating HETs' behavior have been developed, most of them fluid or hybrid. All of them share a R, Z geometry and fail to reproduce the experimental data properly, see e.g. [25]. However, the first implicit kinetic model developed at the Ecole Polytechnique reproduced many HET plasma properties without the need for any external knob [15]. In spite of some lacking, such as secondary electron emission at the walls which are not taken into account due to the chosen z, θ geometry, this model indicates that the large electron azimuthal drift velocity that inherently exists in the $\boldsymbol{E} \times \boldsymbol{B}$ discharge of HETs could be responsible for an instability that gives rise to plasma turbulence. This high frequency instability is particularly efficient in terms of diffusion and could be at the origin of electron transport across the magnetic field.

Up to now, experimental data were lacking to be compared with numerical outcomes of this kinetic model. Indeed, experimental macroscopic data, such as discharge current or thrust, is not enough to characterize HET underlying physical principles. Thanks to the ion VDFs presented in this paper, we were able to perform a direct comparison between theoretical and experimental ion VDF. In figure 10, we compare computed and measured on-axis mean velocity and velocity dispersion

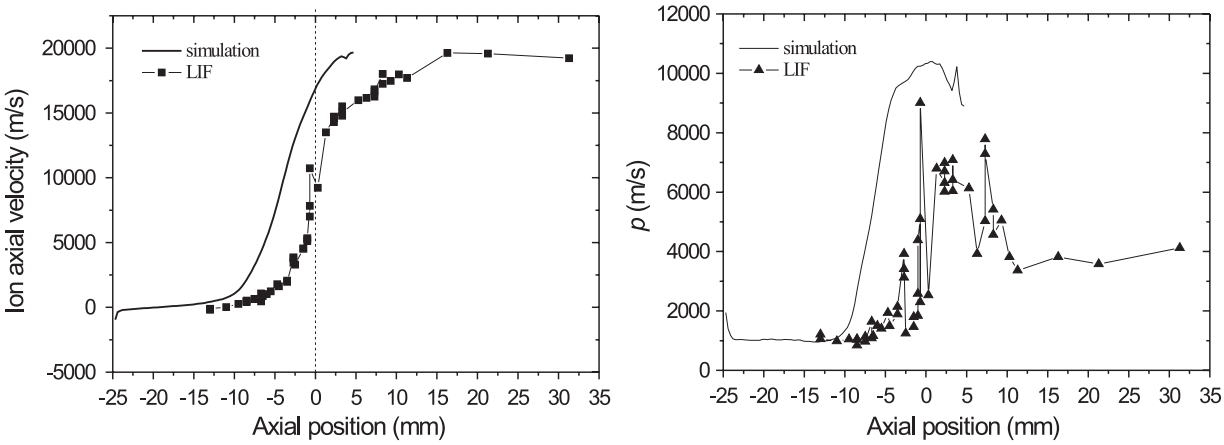

Figure 10. Comparison between numerical outcomes of a kinetic model developed by Adam *et al* [15] and experimental results for the PPS100 normal operating conditions (300 V, 5 mg s^{-1} and 4.5 A in coils). Left: on-axis profile of the ion mean velocity. Right: on-axis profile of the dispersion (p parameter).

(p parameter) obtained under normal operating conditions. Of course, since experimental measurements were time-averaged, it is not possible to comment on the ion dynamic predicted by the model, but when averaged, we can see that measured and predicted ion flow properties are quite similar. The axial velocity profiles are the same, even though there is a shift in position between the two curves. This is due to the boundary of the computation domain. The latter stretches from the anode to 5 mm ahead of the thruster channel exit [15]. This constraint warrants the magnetic field being purely radial in the whole simulation domain. In terms of potential, the boundaries are the following: 300 V at the anode and 0 V at $z = 5$ mm. Yet, experimental measurements show ions reach the maximum acceleration potential beyond $z = 5$ mm. Calculations and experiments provide the same maximum value of the ion axial velocity around 19 600 m s^{-1}, below the highest achievable velocity, i.e. 21 000 m s^{-1}. This result means that the applied potential is not fully converted into axial motion. Part of the supplied energy is spent on ionization. Another part of it is lost in radial motion and in plasma–wall interactions. The development of the VDF width along the channel axis calculated with the kinetic model is qualitatively in agreement with the measured profiles, as can be seen in figure 10. The Xe$^+$ ion VDFs are predicted to be broad. The highest value of the velocity dispersion is reached when the ion accelerating potential is equal to ∼205 eV according to simulations and to ∼185 eV according to measurements, see figure 10. Besides, kinetic modeling confirms that the ion velocity dispersion is maximum at the end of the ionization zone [15]. Finally, the PIC simulations predict the creation of very slow and very fast Xe$^+$ ions, as can be seen in figure 11. Such ions are created whereas any charge exchange mechanism is included in the model; they originate from fast oscillations of the electric field.

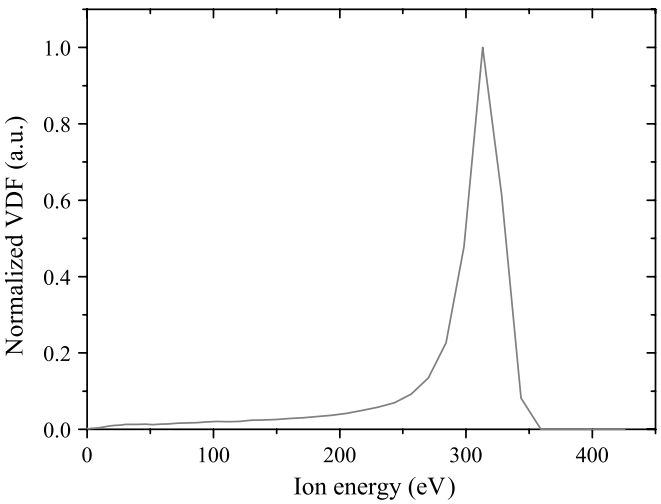

Figure 11. VDF of Xe$^+$ ions at the end of the acceleration layer computed from a kinetic model for the PPS100 fired under normal operating conditions (see figure 10) [15].

8. Conclusion

Works reviewed in this contribution reveal several important facts about the physics of a HET. The acceleration zone is relatively narrow and most of the potential drop occurs outside the thruster channel. Both the applied voltage and the magnetic field have an impact upon the accelerating potential profile. When increasing the magnitude of U_d or B the fraction of the potential inside the thruster channel increases. The spatial extent of the electric field drops when U_d is ramped up, whereas it stays roughly constant when B is increased. Observed trends originates from a change in electron transport properties, however, the physics at hand is not yet understood. Furthermore, a critical examination of the development along the channel axis of the ion velocity dispersion shows in an unambiguous way that ionization and acceleration processes are deeply entangled. This study also confirms the existence of very slow and very fast ions, i.e. ions of which the kinetic energy is much larger than the applied potential. Slow and fast Xe$^+$ ions are a direct consequence of the time evolution of the potential map. Finally, LIF measurements support the outcomes of a z–θ kinetic model that predicts the crucial role of plasma turbulence on anomalous cross-field electron mobility. In particular, numerical simulations and experiments agree on the velocity and velocity dispersion profiles as well as on the creation of slow and fast ions.

From now on a series of news experiments can be envisaged in order to collect complementary data and to gain in the understanding of the physics of the $\boldsymbol{E} \times \boldsymbol{B}$ discharge of a Hall thruster. Examination of the Xe^+ ion VDF in a high power thruster would allow one to study the effect of size and to analyze ion transport phenomena at high voltage. But, above all, in view of recent discoveries it appears essential to investigate the temporal characteristics of the ion VDF and to compare numerical outcomes with experimental results.

Acknowledgments

This work is carried out in the framework of the joint research program 2759 CNRS/CNES/SNECMA/Universités '*Propulsion Spatiale à Plasma*'.

References

[1] Frisbee R H 2003 *J. Propulsion Power* **19** 1129
[2] Morozov A I and Savelyev V V 2000 Fundamentals of stationary plasma thruster theory *Reviews of Plasma Physics* vol 21 ed B B Kadomtsev and V D Shafranov (Dordrecht: Kluwer/New York: Plenum) p 203 and references herein
[3] Mazouffre S, Lazurenko A, Lasgorceix P, Dudeck M, d'Escrivan S and Duchemin O 2007 *Proc. 7th Int. Symp. on Launcher Technologies (Barcelona, Spain)* paper O-25 and references herein
[4] Kim V, Kozlov V, Lazurenko A, Popov G, Skrylnikov A, Clauss C, Day M and Sancovic J 1998 *Proc. 34th Joint Propulsion Conf. and Exhibit (Cleveland, OH)* AIAA paper 98-3335
[5] Manzella D H, Jacobson D T and Jankovsky R S 2001 *Proc. 37th Joint Propulsion Conf. and Exhibit (Salt Lake City, UT)* AIAA paper 01-3774
[6] Martinez-Sanchez M and Pollard J E 1998 *J. Propulsion Power* **14** 688
[7] Zhurin V V, Kaufman H R and Robinson R S 1999 *Plasma Sources Sci. Technol.* **8** R1
[8] Koppel C R, Marchandise F, Prioul M, Estublier D and Darnon F 2005 *Proc. 41st Joint Propulsion Conf. and Exhibit (Tucson, AZ)* AIAA paper 05-3671
[9] Hargus W A Jr and Cappelli M A 2001 *Appl. Phys.* B **72** 961
[10] Dorval N, Bonnet J, Marque J P, Rosencher E, Chable S, Rogier F and Lasgorceix P 2002 *J. Appl. Phys.* **91** 4811
[11] Hargus W A Jr and Nakles M R 2006 *Proc. 42nd Joint Propulsion Conf. and Exhibit (Sacramento, CA)* AIAA paper 06-4991
[12] Gawron D, Mazouffre S, Albarède L and Sadeghi N 2006 *Proc. 42nd Joint Propulsion Conf. and Exhibit (Sacramento, CA)* AIAA paper 06-4473
[13] Smith T B, Ngom B B, Linnell J A and Gallimore A D 2005 *Proc. 41st Joint Propulsion Conf. and Exhibit (Tucson, AZ)* AIAA paper 05-4406
[14] Sadeghi N 2004 *J. Plasma Fusion Res.* **80** 767
[15] Adam J C, Héron A and Laval G 2004 *Phys. Plasmas* **11** 295
[16] Boeuf J-P and Garrigues L 1997 *J. Appl. Phys.* **84** 3547
[17] Miller J S, Pullins S H, Levandier D J, Chiu Y-H and Dressler R A 2002 *J. Appl. Phys.* **91** 984
[18] Choueiri E Y 2001 *Phys. Plasmas* **8** 1411
[19] Hagelaar G J M, Bareilles J, Garrigues L and Boeuf J-P 2003 *J. Appl. Phys.* **93** 67
[20] Bareilles J 2002 Modélisation 2D hybride d'un propulseur à effet Hall pour satellites *PhD Thesis* University of Toulouse, France (in French)
[21] King L B and Gallimore A D 2004 *J. Propulsion Power* **20** 228
[22] Lazurenko A, Albarède L and Bouchoule A 2006 *Phys. Plasmas* **13** 083503
[23] Kurzyna J, Mazouffre S, Lazurenko A, Albarède L, Bonhomme G, Makowski K, Dudeck M and Peradzynski Z 2005 *Phys. Plasmas* **12** 123506
[24] Raitses Y, Staack D, Keidar M and Fisch N J 2005 *Phys. Plasmas* **12** 057104
[25] Scharfe M K, Gascon N, Cappelli M A and Fernandez E 2006 *Phys. Plasmas* **13** 083505